JVI Journals.ASM.org

A Conformational Transition Observed in Single HIV-1 Gag Molecules during *In Vitro* Assembly of Virus-Like Particles

James B. Munro,[a] Abhinav Nath,[b] Michael Färber,[a] Siddhartha A. K. Datta,[c] Alan Rein,[c] Elizabeth Rhoades,[b] Walther Mothes[a]

Department of Microbial Pathogenesis, Yale University School of Medicine, New Haven, Connecticut, USA[a]; Department of Molecular Biophysics and Biochemistry, Yale University, New Haven, Connecticut, USA[b]; HIV Drug Resistance Program, National Cancer Institute, National Institutes of Health, Frederick, Maryland, USA[c]

ABSTRACT

The conformational changes within single HIV-1 Gag molecules that occur during assembly into immature viruses are poorly understood. Using an *in vitro* assembly assay, it has been proposed that HIV-1 Gag undergoes a conformational transition from a compact conformation in solution to an extended rod-like conformation in virus-like particles (VLPs). Here we used single-molecule Förster resonance energy transfer (smFRET) to test this model by directly probing the conformation of single HIV-1 Gag molecules. We demonstrate that monomeric HIV-1 Gag lacking the p6 domain and the N-terminal myristoyl moiety is found in solution predominantly in a compact conformation. Gag in this conformation, and in the presence of nucleic acid, assembles into 30-nm-diameter particles. However, with the addition of inositol hexakisphosphate, Gag adopts a linear conformation and assembles into full-sized ~100-to-150-nm-diameter VLPs. Parallel fluorescence correlation spectroscopy measurements show that this conformational transition occurs early in the assembly process when Gag oligomers are small, perhaps as early as upon dimerization. Thus, smFRET measurements confirm that HIV-1 Gag transitions from a compact to a linear conformation during the formation of VLPs. Our results are consistent with a model whereby binding of HIV-1 Gag to phosphoinositides at the plasma membrane stabilizes an extended conformation and promotes oligomerization into the radially aligned immature capsid.

IMPORTANCE

The establishment of single-molecule fluorescence techniques reveals the conformational state of individual HIV-1 Gag molecules prior to and during *in vitro* assembly into virus-like particles. The data demonstrate that Gag in distinct conformations forms particles with different morphologies. In the compact conformation, in the presence of nucleic acid, Gag forms spherical particles of a diameter of approximately 30 nm. In the extended conformation, Gag forms spherical virus-like particles of approximately 100-nm diameter. The adoption of the extended conformation required the presence of inositol hexakisphosphate in addition to nucleic acid. Our results are consistent with a model whereby binding of HIV-1 Gag to phosphoinositides at the plasma membrane stabilizes an extended conformation and promotes oligomerization into the radially aligned immature capsid.

The replication of human immunodeficiency virus (HIV-1) requires the assembly of new virions at the plasma membrane of infected cells. Virus assembly is driven by the viral Gag polyprotein precursor that alone can form and release immature virus-like particles (VLPs) (1–7). In the immature capsid, Gag proteins are aligned radially to form a spherical shell around a dimeric viral RNA genome. Gag is comprised of four main independently folded domains (1, 3–5, 8). The N-terminal matrix (MA) domain targets Gag to the plasma membrane by way of a myristoyl modification and a basic patch of residues that interacts with phosphoinositides. The capsid (CA) domain drives multimerization through dimeric and hexameric interaction with neighboring Gag molecules, giving rise to a hexagonal lattice. The nucleocapsid (NC) domain contains a pair of zinc-knuckle motifs that recruit the dimeric genome. Finally, a C-terminal p6 peptide recruits the cellular endosomal sorting complexes required for transport (ESCRT) machinery, which promotes the final membrane scission event needed to release the assembled virus into the extracellular space.

The molecular events that underlie the assembly of individual Gag molecules into immature virus particles are poorly understood. To gain insights into these events, an *in vitro* assembly assay has been applied in which purified monomeric HIV-1 Gag assembles into VLPs in the presence of nucleic acid and inositol phosphate, which are the same size as authentic immature HIV-1 virions (9, 10). Structural studies have shown that HIV-1 Gag lacking most of the matrix domain and the p6 domain assembles into VLPs with a Gag lattice that is identical to that of authentic immature virions (11, 12). To more faithfully reflect the behavior of the full-length Gag protein that assembles into immature virions *in vivo*, the matrix protein was included in the present study. Given that the Gag protein used here is closer to authentic Gag than the protein studied structurally, we expect that the native lattice is maintained in the VLPs. Interestingly, Gag lacking the p6 domain and the N-terminal myristoyl moiety (GagΔmyrΔp6) in the presence of nucleic acid assembles into 30-nm-diameter spherical par-

Received 13 November 2013 **Accepted** 2 January 2014

Published ahead of print 8 January 2014

Editor: W. I. Sundquist

Address correspondence to James B. Munro, james.munro@yale.edu, or Walther Mothes, walther.mothes@yale.edu.

doi:10.1128/JVI.03353-13

ticles (9). And the presence of inositol hexakisphosphate (IP6) is required to form VLPs of the correct 100-to-150-nm-diameter size (10, 13, 14). The interaction of MA with IP6 presumably mimics the interaction of Gag with the phosphoinositides found in the plasma membrane (14–17).

The observation of 30- and-100-nm-diameter particles indicates that HIV-1 Gag must be conformationally dynamic. Electron tomography has shown that Gag molecules are radially aligned in the immature virus particle in their fully extended ~20-nm-diameter conformation (12, 18). Thus, the *in vitro* formation of small 30-nm-diameter particles in the absence of IP6 suggests that Gag can also assemble in an alternative, more compact conformation. Further biophysical characterizations of Gag have focused on a mutant form that is deficient in multimerization but which maintains other essential features of wild-type Gag (13). Hydrodynamic and small-angle neutron scattering (SANS) experiments indicated that the mutant as well as wild-type Gag adopts a compact conformation in solution (13, 19). Using the existing structures of the domains of Gag, structural models were developed which suggested a folded Gag conformation in which the N-terminal MA domain was proximal to the C-terminal NC domain (13). These models depict a Gag conformation dramatically different from the extended linear structure observed in electron micrographs of the immature capsid. Thus, a large-scale conformational change in Gag appears to be critical during the formation of VLPs.

Here, we used confocal single-molecule Förster resonance energy transfer (smFRET) to directly probe the conformation of individual HIV-1 Gag molecules during *in vitro* assembly of VLPs. Parallel fluorescence correlation spectroscopy (FCS) measurements provided insight into the size of the assemblies. We show that monomeric HIV-1 Gag in solution exists in equilibrium between a compact conformation in which the N and C termini are proximal and an extended conformation, with the compact conformation being predominant. In this compact conformation, and in the presence of nucleic acid, Gag assembles into 30-nm-diameter particles. However, with the addition of inositol hexakisphosphate, Gag adopts a linear conformation and assembles into full-sized ~100- to 150-nm-diameter VLPs. FCS measurements show that the transition in Gag conformation from the compact state to the linear state occurs early in the assembly process while the oligomers remain small. Thus, smFRET measurements of conformational changes within single HIV-1 Gag molecules directly confirm a conformational change that is critical during the formation of VLPs. Our *in vitro* results are consistent with a model whereby binding of HIV-1 Gag molecules to phosphoinositides at the plasma membrane would stabilize an extended conformation and promote oligomerization into the immature capsid where Gag molecules are radially aligned.

MATERIALS AND METHODS

All reagents were purchased from Sigma unless otherwise noted.

Purification of Gag protein. Wild-type HIV-1 Gag lacking the p6 domain was cloned into the pET11c vector (Novagen) (20) and expressed in *Escherichia coli* BL21(DE3) CodonPlus RIPL cells (Agilent Technologies) by growth to an optical density at 650 nm (OD_{650}) of 0.5 at 37°C followed by addition of 0.4 mM isopropyl-β-D-1-thiogalactopyranoside and growth for an additional 4 h. Purification of overexpressed protein was performed as described previously (21). To facilitate purification of the tagged Gag proteins during fluorescent labeling, a polyhistidine tag was introduced onto the N terminus through PCR, replacing the GARAS residues (Fig. 1A). Enzymatic fluorescent labeling required the additional introduction of the S6 peptide onto the C terminus of Gag through PCR. For the introduction of a second fluorophore, the A1 peptide was inserted either onto the N terminus of Gag, immediately following the polyhistidine tag, or adjacent to the protease cleavage site between the MA and CA domains by overlap-extension PCR.

The modified Gag proteins were expressed as described for wild-type Gag. Cells from 1 liter of culture were lysed by the use of a French press in Purification Buffer (20 mM Tris-HCl [pH 8], 1 M NaCl, 10 mM β-mercaptoethanol, 1 mM phenylmethylsulfonyl fluoride, 10% glycerol, 1% Igepal CA-630) with 20 mM imidazole (pH 8). Gag was bound to 4 ml of nickel-nitrilotriacetic acid (Ni-NTA) resin (Qiagen) preequilibrated in the same buffer. The column was washed with 12 ml of the same buffer, followed by washing with 12 ml Purification Buffer–50 mM imidazole (pH 8). Gag was eluted from the column in 0.5-ml fractions of Purification Buffer–300 mM imidazole (pH 8). The fractions containing protein were identified by Bradford Assay (Bio-Rad), pooled, frozen on liquid nitrogen, and stored at −80°C.

Fluorescent labeling of Gag. AlexaFluor488-maleimide and AlexaFluor594-maleimide were purchased from Invitrogen. The fluorophore-coenzyme A (CoA) conjugates (Alexa 488-CoA and Alexa 594-CoA) were prepared as described previously (22). The C-terminal S6 peptide was labeled in a reaction mixture containing 1.5 μM Gag-S6, 5 μM Alexa 488-CoA, 1 μM Sfp (a phosphopantetheinyl transferase from *Bacillus subtilis*), and Labeling Buffer (50 mM HEPES [pH 7.5], 10 mM $MgCl_2$, 1 M NaCl, 1% glycerol, 0.1% Igepal CA-630). The reaction mixture was incubated at 37°C for 2 h. To purify Gag away from unbound fluorophore, the protein was bound to Ni-NTA resin equilibrated with Purification Buffer and washed with 8 column volumes of the same buffer. The protein was eluted from the column in Purification Buffer–300 mM imidazole (pH 8). Fractions containing labeled protein were identified by eye.

The A1 peptide, either at the N terminus or between the MA and CA domains, was labeled in a subsequent reaction mixture containing 1.5 μM Gag(A488), 5 μM Alexa 594-CoA, 1 μM AcpS (a phosphopantetheinyl transferase from *E. coli*), and Labeling Buffer. The reaction mixture was incubated at 37°C for 2 h. Gag was purified away from unbound fluorophore exactly as before. The dually labeled protein was frozen on liquid nitrogen and stored at −80°C.

In the cases of the dually labeled Gag species, the absorbance of the labeled protein was measured at 280 nm, 495 nm, and 590 nm. The extinction coefficient at 280 nm (74,000 M^{-1} cm^{-1}) and the molecular weight (MW = 54,000) of the Gag protein were estimated using ProtParam. The extinction coefficients and molecular weights of the fluorophores were provided by the manufacturer. This information was used to estimate that approximately 50% of the donor-labeled protein lacked an acceptor.

Formation of VLPs. Full-sized VLPs were formed in a reaction mixture containing 2 μM Gag, 0.5 μM 25-nucleotide polyadenosine ($polyA_{25}$) DNA, 0.3 μM IP6, and Assembly Buffer [20 mM Tris-HCl (pH 8), 100 mM NaCl, 10 μM $ZnSO_4$, 1 mM Tris(2-carboxyethyl)phosphine-HCl]. The 30-nm-diameter particles were formed in the same reaction mixture but lacking IP6. For FCS experiments, 10 nM Gag(A488) was included in the assembly reactions. For smFRET experiments, 50 pM Gag(A488/A594) was included. In all cases, the reaction mixture was incubated at room temperature for 2 h prior to measurement. For measurements on monomeric Gag, fluorescently labeled Gag was diluted into Assembly Buffer to the appropriate concentration in the absence of nucleic acid or IP6.

Acquisition and analysis of FCS and smFRET. FCS and smFRET measurements were made on an Olympus IX-71 inverted microscope as described previously (23). Alexa 488 was excited with a 488-nm-wavelength laser (Newport) focused into the solution containing the fluorescently labeled Gag. For FCS measurements, to minimize blinking of Alexa 488, the fluorophore was excited at 5 μW laser power. The emitted fluo-

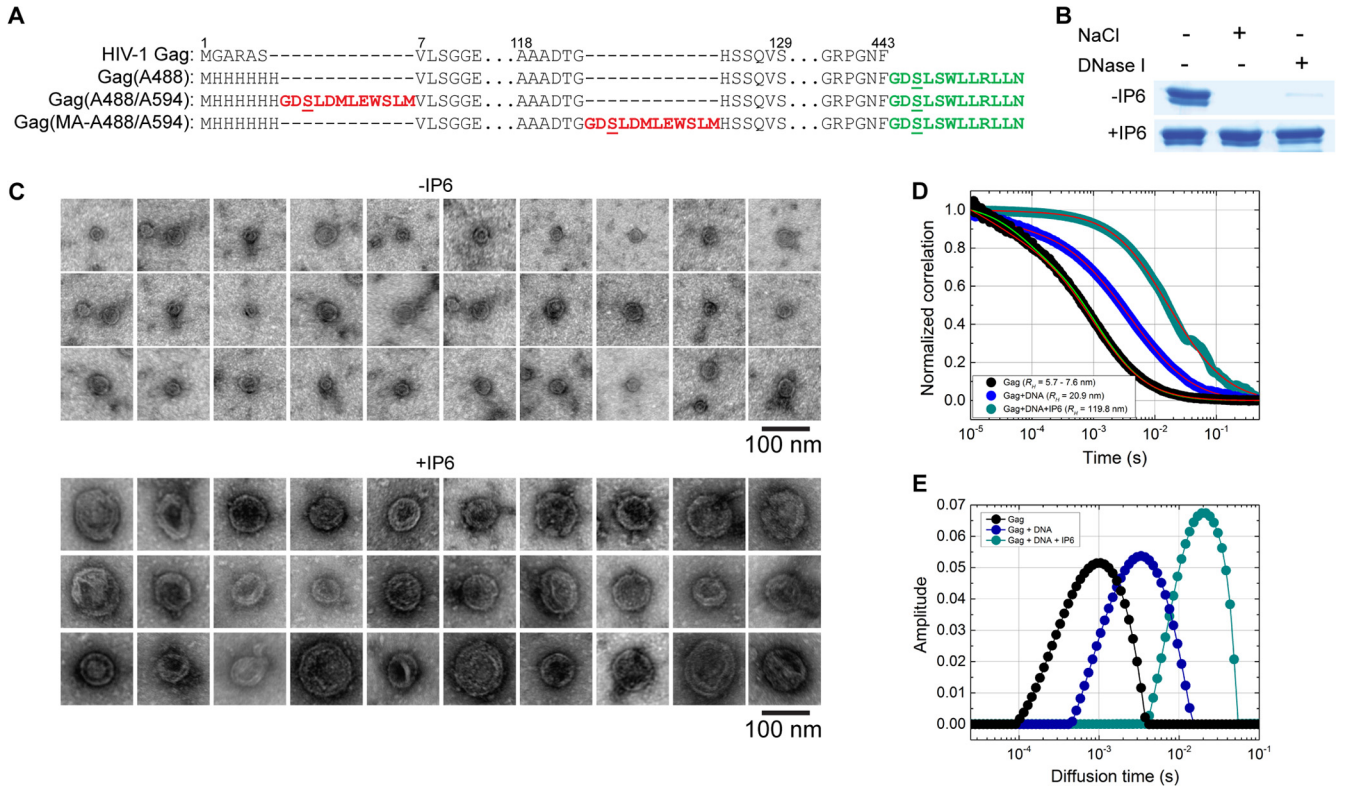

FIG 1 HIV-1 GagΔmyrΔp6 assembles into virus-like particles *in vitro*. (A) Sites of insertion of peptides into HIV-1 Gag for fluorescent labeling. The S6 peptide is shown in green; the A1 peptide is in red. The underlined Ser residue in each tag indicates the site of fluorophore attachment. (B) Coomassie-stained SDS-PAGE gel indicating that HIV-like particles formed in the presence of nucleic acid and IP6 are resistant to treatment with salt or nuclease. (C) Electron micrographs showing that VLPs formed in the presence of nucleic acid alone (top) are smaller than those formed in the presence of nucleic acid and IP6 (bottom). (D) Autocorrelation curves obtained through FCS measurements of 10 nM Gag labeled at the C terminus with Alexa 488 [Gag(A488)] (black); Gag(A488) incubated in the presence of 2 μM unlabeled Gag and 0.5 μM $polyA_{25}$ DNA (blue); and Gag(A488) incubated in the presence of 2 μM unlabeled Gag and 0.5 μM $polyA_{25}$ DNA and 0.3 μM IP6 (cyan). Overlaid in red and green are the fits generated by the maximum entropy method and by fitting to a model of a single diffusing species with a photophysical component, respectively (all fits, $R^2 > 0.9$). The hydrodynamic radii (R_H) estimated from the diffusion times determined through the fitting are indicated (see Materials and Methods). (E) The distribution of diffusion times resulting from maximum entropy fitting of the autocorrelation data in panel D.

rescence was transmitted through a 50-μm-diameter multimode optical fiber to an avalanche photodiode (PerkinElmer).

Autocorrelation curves obtained from monomeric Gag(A488) were fitted to a model of a single diffusing species with an additional photophysical component:

$$G(\tau) = \frac{1}{N(1-A)}(1 - A + A\exp(\tau/\tau_P))(1 + \tau/\tau_D)^{-1}(1 + s^2\tau/\tau_D)^{-1/2} \quad (1)$$

where N is the number of fluorophores in the confocal detection volume, A is the fraction of molecules undergoing the photophysical process, τ_P and τ_D are the time scales of the photophysical and diffusive processes, respectively, and s parameterizes the dimensions of the detection volume. The diffusion time τ_D was used to estimate the hydrodynamic radius R_H of Gag by comparison to values of τ_D and R_H of α-synuclein previously measured by FCS and pulsed-field gradient nuclear magnetic resonance (NMR), respectively (24). The diffusion constant D is given by the formula $D = x^2/4\tau_D$ (where x is the lateral radius of the detection volume). The hydrodynamic radius can then be calculated by the Stokes-Einstein equation, $R_H = k_BT/6\pi\eta D$, where η, k_B, and T are the viscosity of the solution, Boltzmann constant, and the temperature, respectively.

Autocorrelation curves obtained from all samples were fitted using the maximum entropy method (25) implemented in Matlab (Mathworks), similarly to that previously described (26). The data were fitted to a model with a discrete distribution of diffusion times $\tau_{D,i}$:

$$G(\tau) = \sum_i \alpha_i(1 + \tau/\tau_{D,i})^{-1}(1 + s^2\tau/\tau_{D,i})^{-1/2} \quad (2)$$

Here, the α_i values are the amplitudes of the diffusion times and are chosen such that the entropy

$$S = -\sum_i p_i \ln p_i \quad (3)$$

is maximized and

$$\chi^2 = \frac{1}{N}\sum_j r_j^2 \quad (4)$$

is minimized. N is the number of data points being fitted in a given autocorrelation curve, and the r_j values are the residuals of the fit. In the definition of entropy, the p_i values are the normalized diffusion time weights, $p_i = \alpha_i/\Sigma\alpha_i$. Further aspects of the optimization algorithm have been described in detail (25, 26). From the resulting distribution of diffusion times, the weighted average was calculated according to $\langle\tau_D\rangle = \Sigma p_i\tau D_i$, which was used to calculate the diffusion constant and the hydrodynamic radius as described above.

For smFRET experiments, Alexa 488 was excited at 20 μW laser power, and the emitted fluorescence was first split into donor and acceptor channels with a 585-nm-pore-size long-pass dichroic filter (Chroma)

before being transmitted along parallel optical fibers to separate avalanche photodiodes. Photons were collected in 1-ms time bins. Bursts were identified by placing a threshold on the total photon count per bin. FRET efficiency was calculated according to $FRET = n_{acceptor}/(n_{donor} + n_{acceptor})$, where $n_{acceptor}$ and n_{donor} are the numbers of photons per bin in the respective channels after accounting for direct excitation of the acceptor and channel cross talk (27).

Cross-linking of Gag. VLP assembly reactions were initiated exactly as described above for smFRET and FCS measurements. At 5-min intervals, aliquots were removed from the reaction and cross-linked with 2 mM ethylene glycol bis(succinimidylsuccinate) (Thermo Scientific). The cross-linking reaction mixture was incubated for 10 min at room temperature, quenched with 20 mM Tris-HCl (pH 8), and frozen on liquid nitrogen. The cross-linked samples were thawed immediately prior to FCS and smFRET measurements.

TABLE 1 Physical parameters derived from FCS measurements

Target	Diffusion time (ms)	Diffusion constant ($\mu m^2/s$)	Hydrodynamic radius (nm)
Gag (single diffusing species)[a]	1.05 ± 0.01	37.9 ± 0.5	5.7 ± 0.1
Gag (maximum entropy)[b]	1.39 ± 0.01	28.7 ± 0.4	7.6 ± 0.1
Gag + DNA[b]	3.81 ± 0.02	10.4 ± 0.1	20.9 ± 0.1
Gag + DNA + IP6[b]	21.85 ± 0.07	1.82 ± 0.01	119.8 ± 0.4

[a] Data were determined by fitting the autocorrelation curve to a model of a single diffusing species with a photophysical component.
[b] Data were determined by fitting the autocorrelation curve with the maximum entropy method.

RESULTS

Generation of fluorescently labeled Gag. smFRET methods are uniquely positioned to monitor the conformation of single HIV-1 Gag molecules during virus assembly. Single-molecule fluorescence methods depend on chemical or enzymatic strategies to introduce organic fluorophores into Gag. We therefore used the *in vitro* assembly assay, in which GagΔmyrΔp6 is incubated with nucleic acid and IP6 to assemble into immature HIV-1-like particles with a diameter of 100 to 150 nm (10). Organic fluorophores were attached in a site-specific manner to purified Gag using an enzymatic fluorescent labeling strategy whereby 12-amino-acid peptides are recognized by phosphopantetheinyl transferases that transfer the pantetheinyl moiety of CoA to a serine residue in the peptide (28). We therefore conjugated fluorophores to the pantetheinyl moiety of CoA and fused the 12-amino-acid S6 peptide (GDSLSWLLRLLN) to the C terminus of Gag. Incubation with Sfp resulted in the site-specific attachment of a fluorophore onto the C terminus of Gag (Fig. 1A). Similarly, the 12-amino-acid A1 peptide (GDSLDMLEWSLM) fused to the N terminus of Gag, or inserted between MA and CA, allowed site-specific labeling using AcpS (Fig. 1A).

GagΔmyrΔp6 carrying N and C-terminal labeling peptides was purified from *E. coli* and labeled at the C terminus with AlexaFluor488 [Gag(A488)]. Incubation of Gag(A488) with excess wild-type Gag and 25-nucleotide polyadenosine ($polyA_{25}$) DNA in the absence of IP6 led to the formation of particles that were sensitive to incubation with elevated salt or nuclease levels (Fig. 1B). In contrast, in the additional presence of IP6, Gag assembled into particles that were resistant to salt and nuclease (Fig. 1B). As anticipated, electron micrographs of the assembled particles confirmed that the two particles were morphologically different (10). In the absence of IP6, particles were formed with a diameter of approximately 30 nm, whereas approximately 100-nm-diameter particles were formed in the presence of IP6 (Fig. 1C). The conformity of these results with those on untagged Gag (10) indicate that the addition of the labeling peptides did not significantly change the assembly properties of Gag.

Diffusive properties of monomeric Gag and VLPs. We performed FCS measurements to assess the diffusive properties and homogeneity of monomeric Gag in solution. FCS measurements were made on a 10 nM solution of Gag(A488). The average autocorrelation curve from 30 repeats was fitted to a model of a single diffusing species with an additional term to account for fluorophore photophysics (Fig. 1D) (29). This yielded a diffusion time of 1.05 ms, which equates to a hydrodynamic radius of 5.7 nm (see Materials and Methods for details of these calculations) (Table 1). This value is similar to although slightly larger than the hydrodynamic radius previously reported for a modified monomeric Gag (~4-nm radius) (13). The slight discrepancy is likely due to either the addition of the S6 peptide and the A488 fluorophore in the present study or the vastly different experimental methods utilized. In either case, this result indicates that, under the present conditions, the labeled Gag is not prone to aggregation and diffuses as a nearly homogeneous monomeric species. This was expected, given that the present experiments were performed at a concentration 500-fold to 1,000-fold lower than the reported dissociation constant of Gag dimerization (14).

FCS measurements of Gag(A488) incubated with excess unlabeled Gag and $polyA_{25}$ DNA indicated that the protein diffused more slowly and more heterogeneously. The autocorrelation curve was fitted to a continuous distribution of diffusion times using the maximum entropy method (25, 26) to rigorously account for the observed particle heterogeneity. This fitting indicated a distribution with a mean diffusion time of 3.81 ms, and a hydrodynamic radius of 20.9 nm, in approximate agreement with electron micrographs (Table 1 and Fig. 1C to E). Particles formed in the additional presence of IP6 yielded a distribution of diffusion times with a mean of 21 ms, and a hydrodynamic radius of 119.8 nm, which is again in approximate agreement with the electron micrographs (Table 1 and Fig. 1C to E). For comparison, maximum-entropy fitting of the monomeric Gag autocorrelation curve yielded a mean diffusion time of 1.39 ms and a hydrodynamic radius of 7.6 nm. FCS thus provides a means by which to assay the *in vitro* formation of VLPs.

Conformational equilibrium of monomeric Gag. In order to probe the conformation of single HIV-1 Gag molecules using confocal smFRET, we generated Gag labeled at the N terminus with the donor fluorophore Alexa 488 and at the C terminus with the acceptor Alexa 594 Gag(A488/A594) (Fig. 2A, left panel). FRET data were acquired at 50 pM Gag(A488/A594), a concentration 200-fold lower than had been used for the FCS measurements, which had indicated a monomeric species. At these concentrations, each detected burst of photons corresponds to a single labeled Gag molecule freely diffusing through the observation volume. Energy transfer efficiency values calculated from each burst reflect the conformation of Gag(A488/A594) averaged over the typical duration of a transit (~1 ms). The data show two dominant FRET states, consistent with single Gag molecules adopting two distinct conformations (Fig. 2B, left panel). Bulk fluorescence

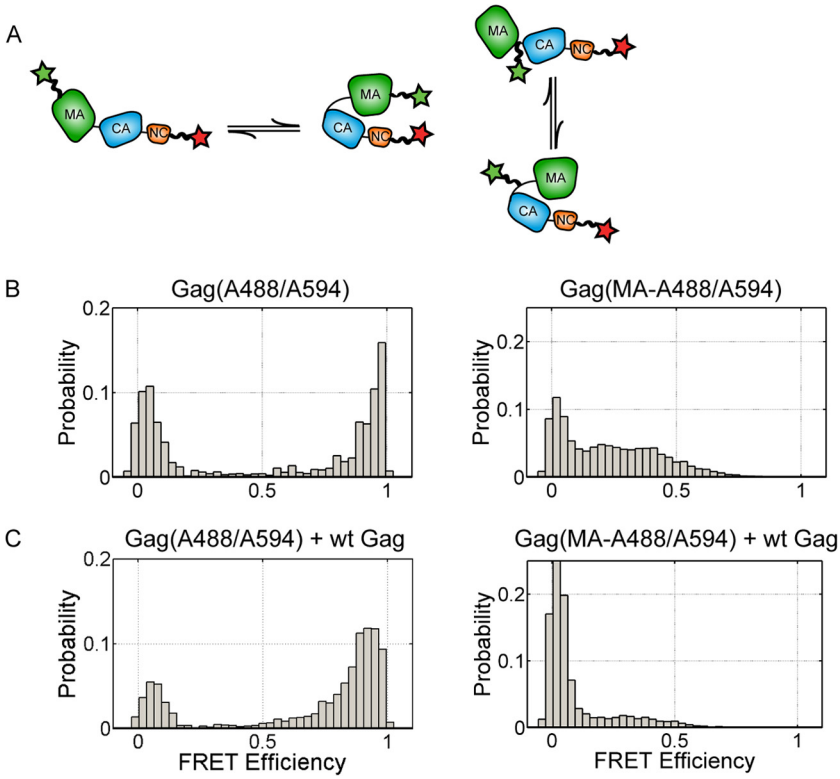

FIG 2 HIV-1 Gag adopts a compact conformation in solution. (A) Putative conformational rearrangement of monomeric Gag. Stars indicate the positions of fluorophores on Gag (green, Alexa 488; red, Alexa 594). (B) Distribution of FRET for monomeric Gag(A488/A594) (50 pM) labeled at the N and C termini (left) and Gag(MA-A488/A594) labeled between MA and CA and at the C terminus (right). The histograms contain 3,403 (left) and 5,340 (right) observations of FRET from single Gag molecules. (C) The same data presented in panel B for labeled Gag in the presence of excess unlabeled Gag (2 μM). The histograms contain 1,559 (left) and 7,390 (right) observations of FRET. wt, wild type.

anisotropy measurements indicated that the different FRET states reflect Gag conformations and not artifacts due to loss of dye motility when bound to Gag (data not shown). The more abundant high-FRET state (>0.9 FRET) is consistent with the N and C termini being proximal, as predicted for a compact, U-shaped conformation of Gag (Fig. 2A, left panel). The lower FRET value of ~0 is consistent with an extended Gag conformation in which the termini are predicted to be as much as 20 nm apart. However, the presence of a 0 FRET peak is a well-known artifact in smFRET measurements of diffusing molecules, arising from molecules labeled with only an active donor fluorophore. Based on the relative levels of absorbance of the labeled protein at 280 nm, 495 nm, and 590 nm, we estimated that 50% of the donor-labeled Gag molecules lacked an acceptor. Thus, this population of Gag molecules cannot entirely account for the 0-FRET peak, and we attribute the remaining events to Gag molecules with an extended conformation. The clear separation between the high- and low-FRET states and the minimal observation of intermediate FRET values in the 0.2 to 0.7 range suggest that the frequency of transition between the two conformations is low and that the time spent transitioning is short with respect to the dwell time in the detection volume. Thus, monomeric Gag prefers a stable compact conformation in solution, although conformations in which the termini are relatively distal remain accessible.

Structural studies indicate an unstructured linker between the MA and CA domains of Gag (30). We thus sought to test if this linker could form a hinge about which MA might rotate, bringing it closer to the N-terminal domain of CA and resulting in a more compact Gag conformation. Such a model was suggested by SANS data (13) and would be consistent with NMR data indicating that MA and CA tumble independently (30). To this end, we moved the A1 peptide from the N terminus to the linker between MA and CA, nine residues N terminal to the viral protease cleavage site (Fig. 1A). The resulting FRET signal indicated an ~0-FRET peak and a broad distribution extending beyond 0.5 FRET (Fig. 2B, right panel). Importantly, the absence of high FRET indicates that the N terminus of CA cannot come within close proximity to the C terminus of Gag; the labeling positions remain distal to one another even in the compact Gag conformation. These data are, as predicted, consistent with a model in which the linker acts as a hinge about which the MA domain can rotate to a position near CA. The intermediate-FRET values are consistent with additional flexibility in Gag beyond that provided by the linker, which can bring the N terminus of CA closer to the C terminus of Gag.

To test if the conformational equilibrium of Gag was influenced by the increased Gag concentration, which has been shown to promote dimerization, FRET data were acquired on Gag(A488/A594) (50 pM) in the additional presence of 2 μM wild-type unlabeled Gag (14). We observed an approximately 20% increase in the occupancy of the high-FRET compact conformation (>0.7 FRET; Fig. 2C, left panel). For the Gag construct with Alexa 488 placed between MA and CA [Gag(MA-A488/A594)], we observed a notable loss in intermediate-FRET configurations (0.2 to 0.7 FRET) in the presence of excess unlabeled Gag (Fig. 2C, right

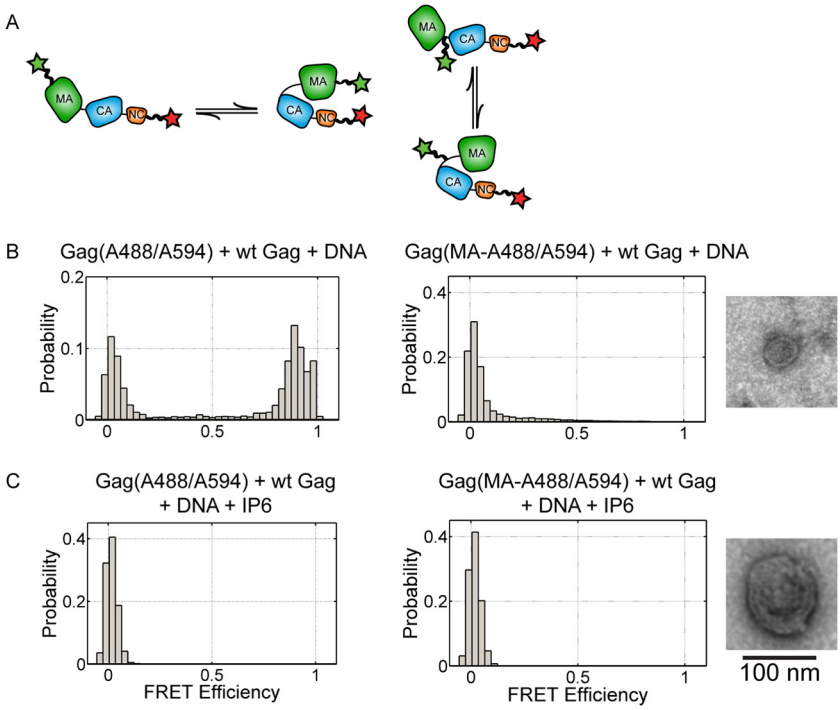

FIG 3 HIV-1 Gag assembles into spherical particles in either the compact or linear conformation. (A) Putative conformational rearrangement of monomeric Gag. Stars indicate the positions of fluorophores on Gag (green, Alexa 488; red, Alexa 594). (B) Distribution of FRET for particles assembled in the presence of excess unlabeled Gag (2 μM) and nucleic acid (left) with Gag(A488/A594) labeled at the N and C termini (50 pM) (left) and Gag(MA-A488/A594) labeled between MA and CA and at the C terminus (50 pM) (center). The histograms contain 3,347 (left) and 8,534 (center) observations of FRET from individual Gag molecules. (Right panels) Representative electron micrograph of the particles formed. (C) The same data as in panel B for particles formed in the additional presence of IP6. The histograms contain 1,020 (left) and 4,223 (center) observations of FRET.

panel). Both observations are consistent with increasing Gag-Gag interactions at higher protein concentrations that stabilize the compact conformation and limit the flexibility of the protein. Alternatively, we cannot rule out the possibility that the conformational landscape observed for dually labeled Gag in the absence of unlabeled Gag may reflect effects of the labeling peptides on Gag conformation which are mitigated in the presence of excess wild-type Gag.

Conformational state of single Gag molecules in VLPs. We next sought to identify the conformation of single Gag molecules within assembled HIV-1 VLPs. Terminally labeled Gag(A488/A594) (50 pM) was incubated with excess wild-type Gag (2 μM) and polyA$_{25}$ DNA in the absence or presence of IP6. Given that up to ~5,000 Gag molecules will assemble into an immature particle, a 40,000-fold excess of unlabeled wild-type Gag will guarantee that, on average, only one labeled Gag molecule will be incorporated into an assembling particle. In the absence of IP6, particles were formed in which a large proportion of Gag was found in a high-FRET state, indicative of a compact conformation (Fig. 3A and B, left panels). Electron micrographs acquired in parallel indicated the formation of spherical particles with a diameter of approximately 30 nm (Fig. 1C and 3B). In the presence of IP6, particles were formed in which the high-FRET configuration was entirely lost (Fig. 3C, left panel). This indicated that Gag had efficiently adopted the extended conformation, as well as validating our interpretation of the 0-FRET peak as corresponding to an extended Gag conformation. Here again, electron micrographs confirmed that full-sized, approximately 100-nm-diameter VLPs had been formed (Fig. 1C and 3C). In the absence of polyA$_{25}$ DNA, but in the presence of IP6, no particles were formed, and no effect on the conformation of Gag was seen compared to the presence of Gag alone (data not shown). Parallel data acquired on Gag with a fluorophore between MA and CA indicated low FRET in both the presence and absence of IP6, again consistent with the linker region between MA and CA functioning as a hinge about which MA rotates (Fig. 3, right panels). Thus, Gag is conformationally dynamic and can assemble in the presence of nucleic acid into spherical particles in either the compact or extended conformation. However, interaction with IP6 and nucleic acid is required for formation of full-sized VLPs in which Gag adopts the extended conformation.

Gag adopts the extended conformation early in the assembly reaction. We next asked when Gag undergoes the transition from the compact to the extended conformation during VLP assembly. To address this issue, we performed smFRET measurements to report on Gag conformation, in parallel with FCS measurements to assess the size of the Gag complexes, during assembly of VLPs. Either dually labeled Gag(A488/A594) (50 pM) or Gag(A488) (10 nM) was incubated with 2 μM unlabeled Gag and IP6, and the assembly reaction was started by addition of polyA$_{25}$ DNA. As shown in Fig. 4, the fluorescence profile from an FCS measurement indicated the steady growth of large bright Gag multimers as observation of the high-FRET compact Gag conformation decreased. The compact conformation was nearly undetectable after 15 min, suggesting that the Gag conformational change occurs early in the assembly reaction.

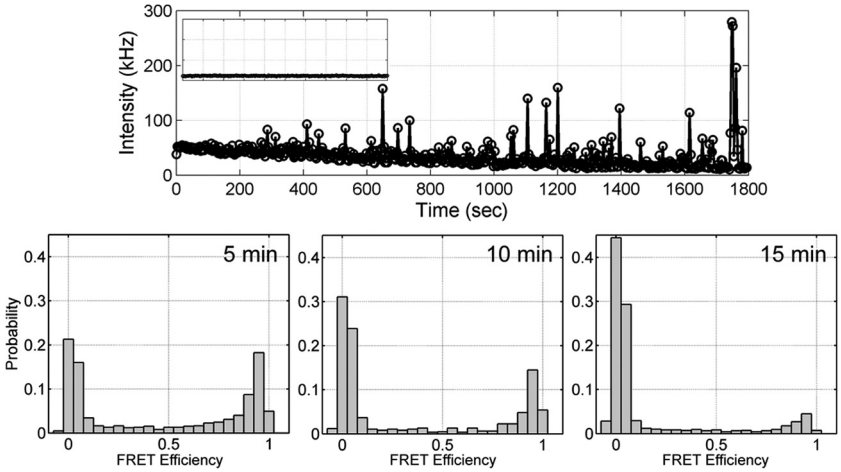

FIG 4 Gag transitions to the linear conformation during assembly of authentic HIV-like particles. (Top panel) Fluorescence profile acquired during the assembly of HIV-like particles in the presence of fluorescent Gag(A488) labeled at the C terminus (10 nM), unlabeled Gag (2 μM), and IP6. The VLP assembly reaction was started by addition of polyA$_{25}$ DNA during data acquisition. Spikes in fluorescence indicate the detection of large, slowly diffusing assemblies. The inset, plotted on the same time and intensity scales, shows the fluorescence profile prior to the addition of polyA$_{25}$ DNA. (Bottom panels) Histograms of FRET values during the indicated intervals of particle assembly for the same reaction with Gag(A488/A594) (50 pM). Each histogram contains 1,051 observations of FRET from individual Gag molecules.

In order to use FCS to assay the size of the Gag multimers formed when Gag transitions to the extended conformation during VLP assembly, we stabilized the intermediate Gag multimers by cross-linking. VLP assembly reactions were halted at 5-min intervals through cross-linking with ethylene glycol bis(succinimidylsuccinate) (EGS) followed by immediate freezing on liquid nitrogen. The cross-linked samples were thawed immediately prior to parallel FRET and FCS measurements. The FRET histograms indicated a loss of the high-FRET compact Gag conformation within 15 min (Fig. 5, left panels). The corresponding FCS data showed no further growth of particles, indicating that the cross-linking halted the VLP assembly process. Fitting the FCS data by the maximum entropy method indicated that after 5 min, the fixed Gag had diffusive properties indistinguishable from that of the monomeric Gag shown in Fig. 1, with a diffusion time of 1.07 ms and a hydrodynamic radius of 5.9 nm. After 10 min, the diffusion time had increased to 1.16 ms, indicating a hydrodynamic radius of 6.4 nm. And after 15 min, when high FRET was nearly undetectable, the diffusion time was 1.30 ms and the hydrodynamic radius was 7.1 nm. No further VLP assembly of the cross-linked samples could be detected during acquisition of the FCS data, indicating that the cross-linking had halted the assembly reaction.

The molecular weight of the diffusing species is approximately proportional to the cube of the hydrodynamic radius (MW = $\sim R_H^3$) (31). We therefore expected that dimeric Gag would diffuse with a hydrodynamic radius on the order of 7.2 nm. The FCS data presented here indicate that the Gag assemblies are on average dimeric after 15 min ($MW_{15\ min}/MW_{5\ min} = [R_{H,15\ min}/R_{H,5\ min}]^3 \approx 1.7$). Thus, the transition from the compact to the extended Gag conformation occurs early in the VLP assembly pathway, perhaps as early as upon dimerization.

DISCUSSION

We have established smFRET methods that allowed us to directly measure the conformational state of single Gag molecules prior to and during *in vitro* assembly into VLPs. In agreement with previous results, we find that monomeric Gag prefers a compact conformation in which the termini are proximal (13, 19). In addition, we document the ability of Gag in distinct conformations to form particles of different morphologies. In the compact conformation, in the presence of polyA$_{25}$ DNA, Gag forms spherical particles of a diameter of approximately 30 nm. In the extended conformation, Gag forms spherical VLPs of approximately 100-nm diameter. The adoption of the extended conformation required the presence of IP6 in addition to that of nucleic acid.

We have established single-molecule fluorescence assays that allow us to monitor the conformation of individual Gag molecules during assembly into VLPs. To what extent these *in vitro* studies apply to assembly in living cells is unknown and depends on the future implementation of single-molecule methods in living cells. The existence of the conformational transition of Gag from the compact to the extended conformation *in vitro* indicates that it must be tightly regulated *in vivo* since only the large-diameter VLPs have been reported in cells. Assembly may begin with interactions between Gag and nucleic acid in the cytoplasm, an environment where the Gag concentration is likely low compared to *in vitro* VLP assembly conditions. Interaction with nucleic acid causes an effective local increase in Gag concentration, which stabilizes the compact conformation. Efficient targeting of the Gag-nucleic acid complex to the plasma membrane must then occur in order to prevent the 30-nm-diameter particles from forming. Indeed, Gag binding to nucleic acid promotes targeting of Gag to the plasma membrane (32). Once genome-bound Gag forms interactions with phosphoinositides in the plasma membrane, and with other Gag proteins, the extended conformation would be stabilized and full-sized immature virions are formed (33, 34). If Gag were to remain in the cytoplasm following interaction with nucleic acid, one would expect 30-nm-diameter particles to accumulate. This is consistent with a report that high-order Gag multimers are predominantly found at the plasma membrane and that the vast majority of Gag in the cytoplasm is monomeric or dimeric

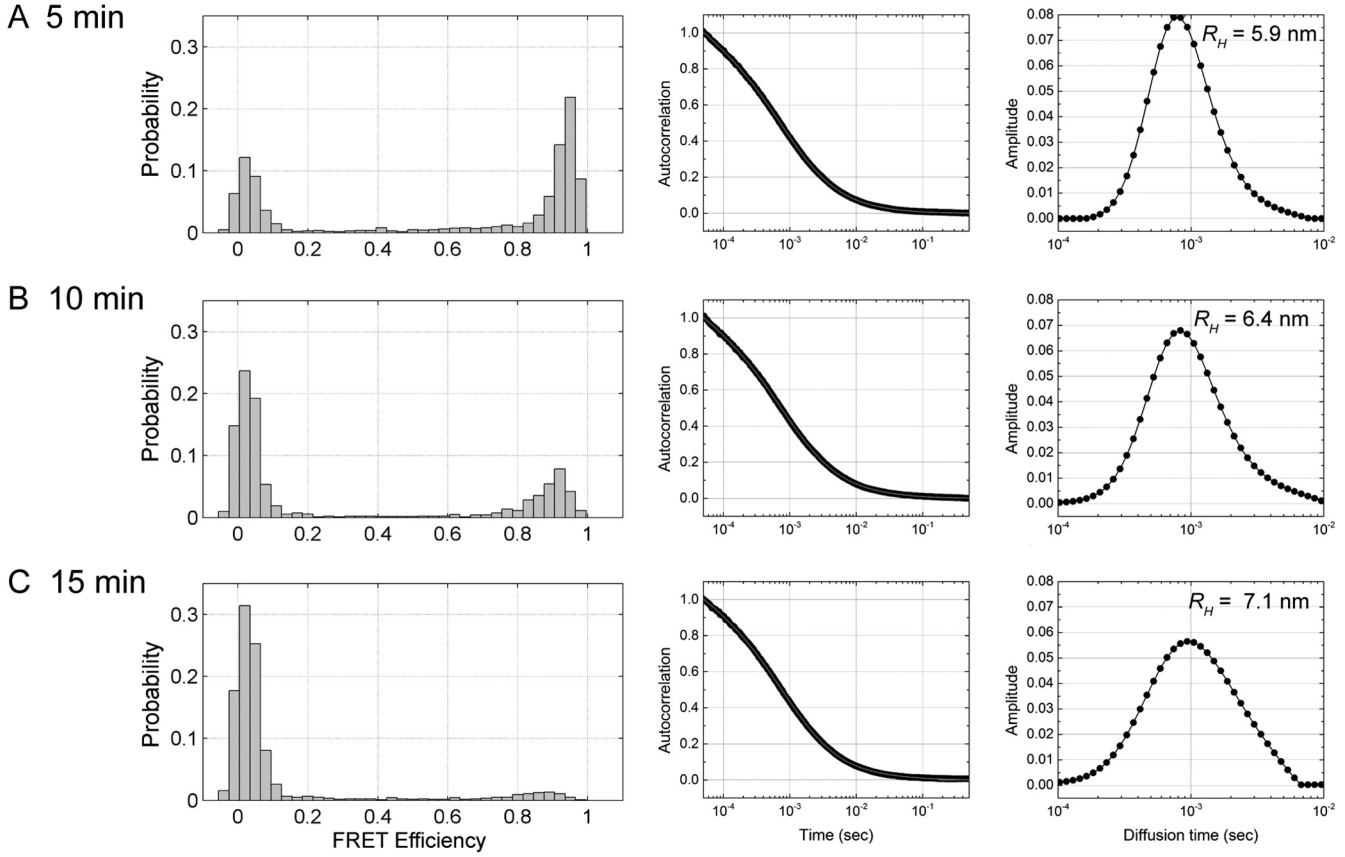

FIG 5 Linearization of Gag occurs early in the assembly process. HIV-like particle assembly reactions that included unlabeled Gag, fluorescent Gag(A488/A594) labeled at the N and C termini, nucleic acid, and IP6 were cross-linked with EGS at the 5 (A)-, 10 (B)-, and 15 (C)-min time points. FRET histograms (left panels), autocorrelation curves with the fit overlaid in red (center panels), and the distributions of diffusion times obtained from maximum entropy fitting (right panels) are shown. The FRET histograms contain 2,453, 1,221, and 1,199 observations of FRET for the 5-, 10-, and 15-min time points, respectively.

(35). Only under conditions of overexpression of Gag containing the G2A mutation at the myristoylation site have full-sized VLPs been found in the cytoplasm; still, no 30-nm-diameter particles were observed (36). This may indicate that, at high expression levels, either an alternative ligand or cytoplasmic membranes can also favor the extended conformation of Gag in the cytoplasm; such small particles might also be difficult to detect in thin sections of the cytoplasm.

We have also shown that the transition from the compact to the extended conformation occurs early in the assembly process of VLPs, perhaps as early as upon dimerization. Thus, the adoption of an extended Gag conformation requires interaction with nucleic acid and IP6 and is stabilized by at least one other Gag molecule (19). This is in agreement with previous observations using neutron reflectivity measurements that Gag bound to small nucleic acids (~7 nucleotides) and that membranes can adopt the extended conformation, although assembly of the immobilized Gag molecules does not occur (19). In the absence of any one of these factors, the compact conformation dominates. This would suggest that the monomeric and dimeric Gag species that are found in the cytoplasm during viral assembly would be in the compact conformation (35). Only upon interaction of Gag with its genome and phosphoinositides at the plasma membrane, combined with local enrichment in lipid microdomains, would transition to the extended conformation occur and permit the assembly of the immature Gag lattice. Future determination of Gag conformation in living cells will be required to verify this model.

ACKNOWLEDGMENTS

This work was supported in part by the Intramural Research Program of the NIH, National Cancer Institute, Center for Cancer Research, to A.R., by NIH grant R21AI096999 to W.M. and E.R., and by a grant from the Irvington Fellowship Program of the Cancer Research Institute to J.B.M.

We declare that we have no conflicts of interest.

REFERENCES

1. **Ganser-Pornillos BK, Yeager M, Pornillos O.** 2012. Assembly and architecture of HIV. Adv. Exp. Med. Biol. **726:**441–465. http://dx.doi.org/10.1007/978-1-4614-0980-9_20.
2. **Lu K, Heng X, Summers MF.** 2011. Structural determinants and mechanism of HIV-1 genome packaging. J. Mol. Biol. **410:**609–633. http://dx.doi.org/10.1016/j.jmb.2011.04.029.
3. **Bieniasz PD.** 2009. The cell biology of HIV-1 virion genesis. Cell Host Microbe **5:**550–558. http://dx.doi.org/10.1016/j.chom.2009.05.015.
4. **Adamson CS, Freed EO.** 2007. Human immunodeficiency virus type 1 assembly, release, and maturation. Adv. Pharmacol. **55:**347–387. http://dx.doi.org/10.1016/S1054-3589(07)55010-6.
5. **Göttlinger HG.** 2001. The HIV-1 assembly machine. AIDS **15**(Suppl 5)**:** S13–S20.
6. **Rein A, Datta SA, Jones CP, Musier-Forsyth K.** 2011. Diverse interactions of retroviral Gag proteins with RNAs. Trends Biochem. Sci. **36:**373–380. http://dx.doi.org/10.1016/j.tibs.2011.04.001.

7. **Morita E, Sundquist WI.** 2004. Retrovirus budding. Annu. Rev. Cell Dev. Biol. **20:**395–425. http://dx.doi.org/10.1146/annurev.cellbio.20.010403.102350.
8. **Chukkapalli V, Ono A.** 2011. Molecular determinants that regulate plasma membrane association of HIV-1 Gag. J. Mol. Biol. **410:**512–524. http://dx.doi.org/10.1016/j.jmb.2011.04.015.
9. **Campbell S, Rein A.** 1999. In vitro assembly properties of human immunodeficiency virus type 1 Gag protein lacking the p6 domain. J. Virol. **73:**2270–2279.
10. **Campbell S, Fisher RJ, Towler EM, Fox S, Issaq HJ, Wolfe T, Phillips LR, Rein A.** 2001. Modulation of HIV-like particle assembly in vitro by inositol phosphates. Proc. Natl. Acad. Sci. U. S. A. **98:**10875–10879. http://dx.doi.org/10.1073/pnas.191224698.
11. **Briggs JA, Riches JD, Glass B, Bartonova V, Zanetti G, Kräusslich HG.** 2009. Structure and assembly of immature HIV. Proc. Natl. Acad. Sci. U. S. A. **106:**11090–11095. http://dx.doi.org/10.1073/pnas.0903535106.
12. **Briggs JA, Simon MN, Gross I, Kräusslich HG, Fuller SD, Vogt VM, Johnson MC.** 2004. The stoichiometry of Gag protein in HIV-1. Nat. Struct. Mol. Biol. **11:**672–675. http://dx.doi.org/10.1038/nsmb785.
13. **Datta SA, Curtis JE, Ratcliff W, Clark PK, Crist RM, Lebowitz J, Krueger S, Rein A.** 2007. Conformation of the HIV-1 Gag protein in solution. J. Mol. Biol. **365:**812–824. http://dx.doi.org/10.1016/j.jmb.2006.10.073.
14. **Datta SA, Zhao Z, Clark PK, Tarasov S, Alexandratos JN, Campbell SJ, Kvaratskhelia M, Lebowitz J, Rein A.** 2007. Interactions between HIV-1 Gag molecules in solution: an inositol phosphate-mediated switch. J. Mol. Biol. **365:**799–811. http://dx.doi.org/10.1016/j.jmb.2006.10.072.
15. **Ono A, Ablan SD, Lockett SJ, Nagashima K, Freed EO.** 2004. Phosphatidylinositol (4,5) bisphosphate regulates HIV-1 Gag targeting to the plasma membrane. Proc. Natl. Acad. Sci. U. S. A. **101:**14889–14894. http://dx.doi.org/10.1073/pnas.0405596101.
16. **Saad JS, Miller J, Tai J, Kim A, Ghanam RH, Summers MF.** 2006. Structural basis for targeting HIV-1 Gag proteins to the plasma membrane for virus assembly. Proc. Natl. Acad. Sci. U. S. A. **103:**11364–11369. http://dx.doi.org/10.1073/pnas.0602818103.
17. **Shkriabai N, Datta SA, Zhao Z, Hess S, Rein A, Kvaratskhelia M.** 2006. Interactions of HIV-1 Gag with assembly cofactors. Biochemistry **45:**4077–4083. http://dx.doi.org/10.1021/bi052308e.
18. **Wright ER, Schooler JB, Ding HJ, Kieffer C, Fillmore C, Sundquist WI, Jensen GJ.** 2007. Electron cryotomography of immature HIV-1 virions reveals the structure of the CA and SP1 Gag shells. EMBO J. **26:**2218–2226. http://dx.doi.org/10.1038/sj.emboj.7601664.
19. **Datta SA, Heinrich F, Raghunandan S, Krueger S, Curtis JE, Rein A, Nanda H.** 2011. HIV-1 Gag extension: conformational changes require simultaneous interaction with membrane and nucleic acid. J. Mol. Biol. **406:**205–214. http://dx.doi.org/10.1016/j.jmb.2010.11.051.
20. **Gross I, Hohenberg H, Wilk T, Wiegers K, Grättinger M, Müller B, Fuller S, Kräusslich HG.** 2000. A conformational switch controlling HIV-1 morphogenesis. EMBO J. **19:**103–113. http://dx.doi.org/10.1093/emboj/19.1.103.
21. **Datta SA, Rein A.** 2009. Preparation of recombinant HIV-1 gag protein and assembly of virus-like particles in vitro. Methods Mol. Biol. **485:**197–208. http://dx.doi.org/10.1007/978-1-59745-170-3_14.
22. **Yin J, Lin AJ, Golan DE, Walsh CT.** 2006. Site-specific protein labeling by Sfp phosphopantetheinyl transferase. Nat. Protoc. **1:**280–285. http://dx.doi.org/10.1038/nprot.2006.43.
23. **Nath A, Trexler AJ, Koo P, Miranker AD, Atkins WM, Rhoades E.** 2010. Single-molecule fluorescence spectroscopy using phospholipid bilayer nanodiscs. Methods Enzymol. **472:**89–117. http://dx.doi.org/10.1016/S0076-6879(10)72014-0.
24. **Sevcsik E, Trexler AJ, Dunn JM, Rhoades E.** 2011. Allostery in a disordered protein: oxidative modifications to α-synuclein act distally to regulate membrane binding. J. Am. Chem. Soc. **133:**7152–7158. http://dx.doi.org/10.1021/ja2009554.
25. **Skilling J, Bryan RK.** 1984. Maximum entropy image reconstruction: general algorithm. Mon. Not. R. Astr. Soc. **211:**111–124.
26. **Sengupta P, Garai K, Balaji J, Periasamy N, Maiti S.** 2003. Measuring size distribution in highly heterogeneous systems with fluorescence correlation spectroscopy. Biophys. J. **84:**1977–1984. http://dx.doi.org/10.1016/S0006-3495(03)75006-1.
27. **Trexler AJ, Rhoades E.** 2009. alpha-Synuclein binds large unilamellar vesicles as an extended helix. Biochemistry **48:**2304–2306. http://dx.doi.org/10.1021/bi900114z.
28. **Zhou Z, Cironi P, Lin AJ, Xu Y, Hrvatin S, Golan DE, Silver PA, Walsh CT, Yin J.** 2007. Genetically encoded short peptide tags for orthogonal protein labeling by Sfp and AcpS phosphopantetheinyl transferases. ACS Chem. Biol. **2:**337–346. http://dx.doi.org/10.1021/cb700054k.
29. **Widengren J, Mets U, Rigler R.** 1995. Fluorescence correlation spectroscopy of triplet states in solution: a theoretical and experimental study. J. Phys. Chem. **99:**13368–13379. http://dx.doi.org/10.1021/j100036a009.
30. **Tang C, Ndassa Y, Summers MF.** 2002. Structure of the N-terminal 283-residue fragment of the immature HIV-1 Gag polyprotein. Nat. Struct. Biol. **9:**537–543. http://dx.doi.org/10.1038/nsb806.
31. **Lakowicz J.** 2006. Principles of fluorescence spectroscopy, 3 ed. Springer, New York, NY.
32. **Chukkapalli V, Inlora J, Todd GC, Ono A.** 3 April 2013. Evidence in support of RNA-mediated inhibition of phosphatidylserine-dependent HIV-1 Gag membrane binding in cells. J. Virol. http://dx.doi.org/10.1128/JVI.00075-13.
33. **Alfadhli A, Still A, Barklis E.** 2009. Analysis of human immunodeficiency virus type 1 matrix binding to membranes and nucleic acids. J. Virol. **83:**12196–12203. http://dx.doi.org/10.1128/JVI.01197-09.
34. **Chukkapalli V, Oh SJ, Ono A.** 2010. Opposing mechanisms involving RNA and lipids regulate HIV-1 Gag membrane binding through the highly basic region of the matrix domain. Proc. Natl. Acad. Sci. U. S. A. **107:**1600–1605. http://dx.doi.org/10.1073/pnas.0908661107.
35. **Kutluay SB, Bieniasz PD.** 2010. Analysis of the initiating events in HIV-1 particle assembly and genome packaging. PLoS Pathog. **6:**e1001200. http://dx.doi.org/10.1371/journal.ppat.1001200.
36. **O'Carroll IP, Crist RM, Mirro J, Harvin D, Soheilian F, Kamata A, Nagashima K, Rein A.** 2012. Functional redundancy in HIV-1 viral particle assembly. J. Virol. **86:**12991–12996. http://dx.doi.org/10.1128/JVI.06287-11.